



Variations in the summer oceanic $p\text{CO}_2$ and carbon sink in Prydz Bay using the self-organizing map analysis approach

Suqing Xu¹, Keyhong Park², Yanmin Wang³, Liqi Chen¹, Di Qi¹, and Bingrui Li⁴

¹Key Laboratory of Global Change and Marine-Atmospheric Chemistry, Third Institute of Oceanography, Ministry of Natural Resources, Xiamen 361005, P. R. China

²Division of Polar Ocean Sciences, Korea Polar Research Institute, Incheon 21990, South Korea

³Haikou Marine Environment Monitoring Central Station, State Oceanic Administration, Haikou 570100, China

⁴Polar Oceanography Division, Polar Research Institute of China, Shanghai 200136, China

Correspondence: Liqi Chen (chenliqi@tio.org.cn) and Keyhong Park (keyhongpark@kopri.re.kr)

Received: 8 June 2018 – Discussion started: 19 July 2018

Revised: 22 December 2018 – Accepted: 14 January 2019 – Published: 13 February 2019

Abstract. This study applies a neural network technique to produce maps of oceanic surface $p\text{CO}_2$ in Prydz Bay in the Southern Ocean on a weekly 0.1° longitude \times 0.1° latitude grid based on in situ measurements obtained during the 31st CHINARE cruise from February to early March 2015. This study area was divided into three regions, namely, the “open-ocean” region, “sea-ice” region and “shelf” region. The distribution of oceanic $p\text{CO}_2$ was mainly affected by physical processes in the open-ocean region, where mixing and upwelling were the main controls. In the sea-ice region, oceanic $p\text{CO}_2$ changed sharply due to the strong change in seasonal ice. In the shelf region, biological factors were the main control. The weekly oceanic $p\text{CO}_2$ was estimated using a self-organizing map (SOM) with four proxy parameters (sea surface temperature, chlorophyll a concentration, mixed Layer Depth and sea surface salinity) to overcome the complex relationship between the biogeochemical and physical conditions in the Prydz Bay region. The reconstructed oceanic $p\text{CO}_2$ data coincide well with the in situ $p\text{CO}_2$ data from SOCAT, with a root mean square error of $22.14 \mu\text{atm}$. Prydz Bay was mainly a strong CO_2 sink in February 2015, with a monthly averaged uptake of $23.57 \pm 6.36 \text{ TgC}$. The oceanic CO_2 sink is pronounced in the shelf region due to its low oceanic $p\text{CO}_2$ values and peak biological production.

1 Introduction

The amount of carbon uptake occurring in the ocean south of 60°S is still uncertain despite its importance in regulating atmospheric carbon and the fact that the region as a net sink for anthropogenic carbon (Sweeney et al., 2000; Sweeney, 2002; Morrison et al., 2001; Sabine et al., 2004; Metzl et al., 2006; Takahashi et al., 2012). This uncertainty arises from both the strong seasonal and spatial variations that occur around Antarctica and the difficulty of obtaining field measurements in the region due to its hostile weather and remoteness.

Following the Weddell and Ross seas, Prydz Bay is the third-largest embayment in the Antarctic continent. Situated in the Indian Ocean, Prydz Bay is located close to the Amery Ice Shelf to the southwest and the West Ice Shelf to the northeast, with Cape Darnley to the west and the Zhongshan and Davis stations to the east (Fig. 1). In this region, the water depth increases sharply northward from 200 to 3000 m.

The inner continental shelf is dominated by the Amery Depression, which generally ranges in depth from 600 to 700 m. This depression is bordered by two shallow banks ($< 200 \text{ m}$): the Fram Bank and the Four Ladies Bank, which form a spatial barrier for water exchange with the outer oceanic water (Smith and Trégure, 1994). The Antarctic Coastal Current (CoC) flows westward, bringing in cold waters from the east. When the CoC reaches the shallow Fram Bank, it turns north and then partly flows westward, while some of it turns eastward, back to the inner shelf, resulting in the clockwise-rotating Prydz Bay gyre (see Fig. 1). The circulation to the north of the bay is characterized by a large cyclonic gyre, ex-

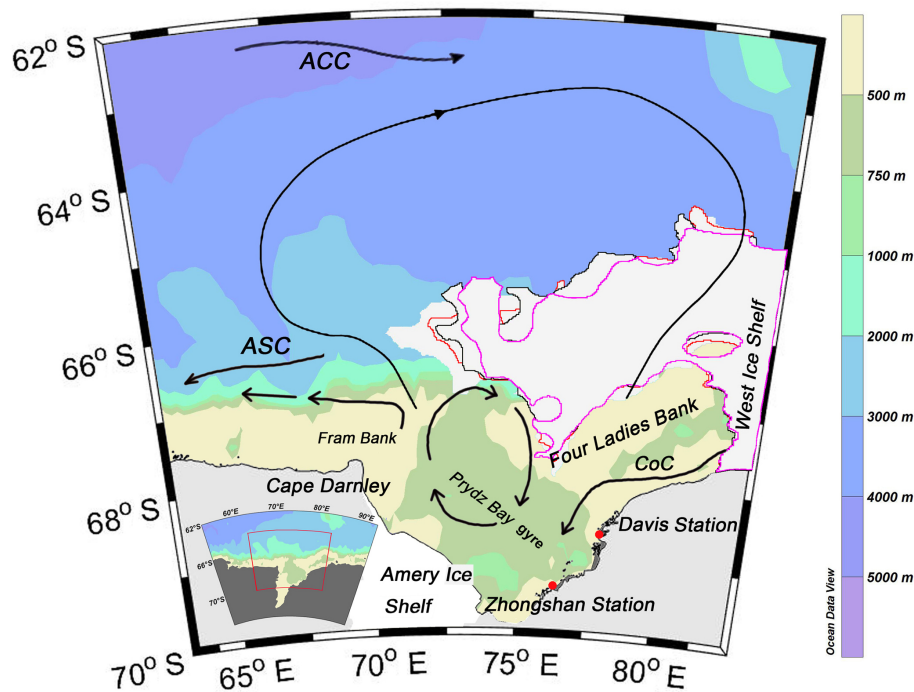


Figure 1. Ocean circulations in Prydz Bay derived from Roden et al. (2013), Sun et al. (2013) and Wu et al. (2017). ASC is the Antarctic Slope Current, CoC is the Antarctic Coastal Current and ACC is the Antarctic Circumpolar Current. During the 4-week cruise, the sea-ice extent varied as indicated by the contoured white areas: the pink line represents week 1 (2–9 February 2015), the black line represents week 2 (10–17 February 2015), the red line represents week 3 (18–25 February 2015) and the unlined white area outside the red contour lines represents week 4 (26 February–5 March 2015).

tending from within the bay to the Antarctic Divergence at approximately 63°S (Nunes Vaz and Lennon, 1996; Middleton and Humphries, 1989; Smith et al., 1984; Roden et al., 2013; Wu et al., 2017). The inflow of this large gyre hugs the eastern rim of the bay and favors the onshore intrusions of the warmer modified Circumpolar Deep Water across the continental shelf break (Heil et al., 1996). Westward flow along the shelf, which is part of the wind-driven Antarctic Slope Current (ASC), supplies water to Prydz Bay.

It has been reported that Prydz Bay is a strong carbon sink, especially in the austral summer (Gibson et al., 1999; Gao et al., 2008; Roden et al., 2013). Moreover, studies have shown that the Prydz Bay region is one of the source regions of Antarctic Bottom Water in addition to the Weddell and Ross seas (Jacobs and Georgi, 1977; Yabuki et al., 2006). Thus, it is important to study the carbon cycle in Prydz Bay. However, the analysis of the temporal variability and spatial distribution mechanism of oceanic $p\text{CO}_2$ in the Prydz Bay is limited to cruises or stations due to its unique physical environment and complicated marine ecosystem (Smith et al., 1984; Nunes Vaz et al., 1996; Liu and Cheng, 2003). To estimate regional sea–air CO_2 fluxes, it is necessary to interpolate between in situ measurements to obtain maps of oceanic $p\text{CO}_2$. However, such an interpolation approach is still difficult, as observations are too sparse over both time

and space to capture the high variability in $p\text{CO}_2$. Satellites do not measure sea surface $p\text{CO}_2$, but they do provide access to the parameters related to the processes that control its variability. The seasonal and geographical variability of surface water $p\text{CO}_2$ is indeed much greater than that of atmospheric $p\text{CO}_2$. Therefore, the direction of sea–air CO_2 transfer is mainly regulated by oceanic $p\text{CO}_2$, and the method of spatially and temporarily interpolating in situ measurements of oceanic $p\text{CO}_2$ has long been used (Takahashi et al., 2002, 2009; Olsen et al., 2004; Jamet et al., 2007; Chierici et al., 2009). In earlier studies, a linear regression extrapolation method was applied to expand cruise data to study the carbon cycle in the Southern Ocean (Rangama et al., 2005; Chen et al., 2011; Xu et al., 2016). However, this linear regression relied simply on either chlorophyll *a* (CHL) or sea surface temperature (SST) parameters. Thus, this method can not sufficiently represent all controlling factors. In this study, we applied self-organizing map (SOM) analysis to expand our observed datasets and estimate the oceanic $p\text{CO}_2$ in Prydz Bay from February to early March 2015.

The SOM analysis, which is a type of artificial neural network, has been proven to be a useful method for extracting and classifying features in the geosciences field, such as trends in (and between) input variables (Gibson et al., 2017; Huang et al., 2017b). The SOM uses an unsupervised learn-

ing algorithm (i.e., with no need for a priori, empirical or theoretical descriptions of input–output relationships), thus enabling us to identify the relationships between the state variables of the phenomena being analyzed, where our understanding of these cannot be fully described using mathematical equations and where applications of knowledge-based models are consequently limited (Telszewski et al., 2009). In the field of oceanography, SOM has been applied for the analysis of various properties of seawater, such as sea surface temperature (Iskandar, 2010; Liu et al., 2006), and chlorophyll concentration (Huang et al., 2017a; Silulwane et al., 2001). Over the past decade, SOM has also been applied to produce basin-scale $p\text{CO}_2$ maps, mainly in the North Atlantic and Pacific oceans, by using different proxy parameters (Lafevre et al., 2005; Friedrich and Oschlies, 2009a, b; Nakaoka et al., 2013; Telszewski et al., 2009; Hales et al., 2012; Zeng et al., 2015; Laruelle et al., 2017). SOM has been proven to be useful for expanding the spatial–temporal coverage of direct measurements or for estimating properties for which satellite observations are technically limited. One of the main benefits of the neural network method over more traditional techniques is that it provides more accurate representations of highly variable systems of interconnected water properties (Nakaoka et al., 2013).

We conducted a survey during the 31st CHINARE cruise in Prydz Bay (Fig. 2). This study aimed to apply the SOM method, combined with remotely sensed data, to reduce the spatiotemporal scarcity of contemporary $p\text{CO}_2$ data and to obtain a better understanding of the capability of carbon absorption in Prydz Bay from 63 to 83° E and 64 to 70° S from February to early March 2015.

The paper is organized as follows. Section 2 provides descriptions of the in situ measurements and SOM methods. Section 3 presents the analysis and discussion of the results, and Sect. 4 presents a summary of this research.

2 Data and methods

2.1 In situ data

The in situ underway $p\text{CO}_2$ values from marine water and the atmosphere were collected during the 31st CHINARE cruise, when the R/V *Xuelong* sailed east–west from the beginning of February to early March 2015 (see Fig. 2a, b). Sea water at a depth of 5 m beneath the sea surface was continuously pumped to the GO system (Model 8050 $p\text{CO}$ measuring system, General Oceanics Inc., Miami FL, USA), and the partial pressure of the sea surface water was measured using an infrared analyzer (LICOR, USA, Model 7000). The analyzer was calibrated every 2.5–3 h using four standard gases supplied by NOAA's Global Monitoring Division at pressures of 88.82, 188.36, 399.47 and 528.92 ppm. The accuracy of the measured $p\text{CO}_2$ data is within $2 \mu\text{atm}$ (Pierrot et al., 2009). Underway atmospheric $p\text{CO}_2$ data were simultane-

ously collected by the GO system. The biological and physical pumps in the ocean (Hardman-Mountford et al., 2009; Bates et al., 1998a, b; Barbini et al., 2003; Sweeney, 2002) are the key factors controlling the variation in sea surface $p\text{CO}_2$. In terms of the physical pumps, the solubility of CO_2 is affected by temperature and salinity, but the biological pumps, such as phytoplankton, take CO_2 up via photosynthesis while organisms release it through respiration (Chen et al., 2011). There are several processes that can influence the distribution of oceanic $p\text{CO}_2$.

Sea-ice melt has a significant impact on the local stratification and circulation in polar regions. During freezing, brine is rejected from ice, thereby increasing the sea surface salinity. When ice begins to melt, fresher water is added into the ocean, thereby diluting the ocean water, i.e., reducing its salinity; thus, changes in salinity record physical processes. In this study, we treat salinity as an index for changes in sea ice. The underway SST and conductivity data were recorded by a conductivity–temperature–depth sensor (CTD, Seabird SBE 21) along the cruise track. Later, sea surface salinity was calculated based on the recorded conductivity and temperature data. The distributions of underway SST and SSS are shown in Fig. 2c and d.

In austral summer, when sea ice started to melt, ice algae were released into the seawater, and the number of living biological species and the amount of primary productivity increased; thus, high chlorophyll *a* values were observed (Liu et al., 2000; Liu and Cheng, 2003). Previous studies have reported that the summer sink in Prydz Bay is biologically driven and that the change in $p\text{CO}_2$ is often well correlated with the surface chlorophyll *a* concentration (Rubin et al., 1998; Gibson et al., 1999; Chen et al., 2011; Xu et al., 2016). The chlorophyll *a* value is regarded as an important controlling factor of $p\text{CO}_2$. Remote sensing data of chlorophyll *a* obtained from MODIS with a resolution of 4 km (<http://oceancolor.gsfc.nasa.gov>, last access: 14 September 2017) were interpolated according to the cruise track (Fig. 2e).

The ocean mixed layer is characterized as having nearly uniform physical properties throughout the layer, with a gradient in its properties occurring at the bottom of the layer. The mixed layer links the atmosphere to the deep ocean. Previous studies have emphasized the importance of accounting for vertical mixing through the mixed layer depth (MLD; Dandonneau, 1995; Lüger et al., 2004). The stability and stratification of this layer prevent the upward mixing of nutrients and limit biological production, thus affecting the sea–air CO_2 exchange. Two main methods are used to calculate the MLD (Chu and Fan, 2010): one is based on the difference criterion, and one is based on the gradient criterion. Early studies suggested that the MLD values determined in the Southern Ocean using the difference criterion are more stable (Brainerd and Gregg, 1995; Thomson and Fine, 2003). Thus, following Dong et al. (2008), we calculated the MLD (see Fig. 2f) based on the difference criterion, in which σ_θ

changed by 0.03 kg m^{-3} . The MLD values at the stations along the cruise were later gridded linearly to match the spatial resolution of the underway measurements.

2.2 SOM method and input variables

We hypothesize that oceanic $p\text{CO}_2$ can be reconstructed using the SOM method with four proxy parameters (Eq. 1): sea surface temperature (SST), chlorophyll a concentration (CHL), mixed layer depth (MLD) and sea surface salinity (SSS).

$$p\text{CO}_2^{\text{sea}} = \text{SOM}(\text{SST}, \text{CHL}, \text{MLD}, \text{SSS}) \quad (1)$$

The SOM is trained to project the input space of training samples to a feature space (Kohonen, 1984), which is usually represented by grid points in 2-D space. Each grid point, which is also called a neuron cell, is associated with a weight vector that has the same number of components as the vector of the input data (Zeng et al., 2017). During SOM analysis, three steps are taken following Nakaoka et al. (2013) to estimate the oceanic $p\text{CO}_2$ fields (see Fig. 3). As the four input environmental parameters (SST, CHL, MLD and SSS) are used to estimate $p\text{CO}_2$ in this study, each input dataset is prepared in 4-D vector form. Here, the SOM analysis was carried out using the MATLAB SOM tool box 2.0 (Vesanto, 2002). This toolbox was developed by the Laboratory of Computer and Information Science at the Helsinki University of Technology and is available from the following web page: <http://www.cis.hut.fi/projects/somtoolbox> (last access: June 2016).

During the training process, each neuron's weight vectors (P_i), which are linearly initialized, are repeatedly trained by being presented with the input vectors (Q_j) of environmental parameters in the SOM training function. Because SOM analysis is known to be a powerful technique with which to estimate $p\text{CO}_2$ based on the nonlinear relationships of the parameters (Telszewski et al., 2009), we assumed that the nonlinear relationships of the proxy parameters are sufficiently represented after the training procedure. During this step, Euclidean distances (D) are calculated between the weight vectors of neurons and the input vectors as shown in Eq. (2), and the neuron with the shortest distance is selected as the winner. This process results in the clustering of similar neurons and the self-organization of the map. The observed oceanic $p\text{CO}_2$ data are not needed in the first step.

$$D(P_i, Q_j) \quad (2)$$

$$= \sqrt{\left\{ \begin{array}{l} (P_{i_SST} - Q_{j_SST})^2 + (P_{i_CHL} - Q_{j_CHL})^2 \\ + (P_{i_MLD} - Q_{j_MLD})^2 + (P_{i_SSS} - Q_{j_SSS})^2 \end{array} \right\}}$$

During the second part of the process, each preconditioned SOM neuron is labelled with an observation dataset of in situ oceanic $p\text{CO}_2$ values, and the labelling process technically

follows the same principles as the training process. The labelling dataset, which consists of the observed $p\text{CO}_2$ and normalized SST, CHL, MLD and SSS data, is presented to the neural network. We calculated the D values between trained neurons and observational environmental datasets. The winner neuron is selected as in step 1 and labelled with an observed $p\text{CO}_2$ value. After the labelling process, the neurons are represented as 5-D vectors.

Finally, during the mapping process, the labelled SOM neurons created by the second process and the trained SOM neurons created by the first process are used to produce the oceanic $p\text{CO}_2$ value of each winner neuron based on its geographical grid point in the study area.

Before the training process, the input training dataset and labelling dataset are analyzed and prospectively normalized to create an even distribution. The statistics and ranges of the values of all variables are presented in Table 1. When the datasets of the four proxy parameters were logarithmically normalized, the skewness values of CHL and MLD changed, especially for the training dataset. The N coverage represents the percentage of the training data that are labelled. The data N coverage values of the training datasets of CHL, MLD and SSS are 82.1 %, 85 % and 81.1 %, respectively, which may be due to their insufficient spatiotemporal coverage and/or bias between the labelling and training datasets. The N coverage of the logarithmic datasets changed to 93.6 % and 98.7 % for CHL and MLD, respectively. Thus, the common logarithms of the CHL and MLD values are used for both the training and labelling datasets to resolve the data coverage issue arising from significantly increasing the data coverage as well as to overcome the weighting issue arising from the different magnitudes between variables (Ultsch and Röske, 2002).

In this study, we construct weekly oceanic $p\text{CO}_2$ maps from February to early March 2015 using four datasets, i.e., SST, CHL, MLD and SSS. Considering the size of our study region, we chose a spatial resolution of 0.1° latitude by 0.1° longitude. For SST, we used daily data from AVHRR-Only (<https://www.ncdc.noaa.gov/oisst>, last access: 22 September 2017) with a $1/4^\circ$ spatial resolution (see Fig. S1 in the Supplement). The CHL data represent the 8-day composite chlorophyll a data from MODIS-Aqua (<http://oceancolor.gsfc.nasa.gov>, last access: 14 September 2017) with a spatial resolution of 4 km (see Fig. S2). We also used the daily SSS and MLD data (see Figs. S3–S4) from the $1/12^\circ$ global analysis and forecast product from the Copernicus Marine Environment Monitoring Service (CMEMS, <http://marine.copernicus.eu/>, last access: 28 September 2017). Sea-ice concentration data are from the daily 3.125 km AMSR2 dataset (Spren et al., 2008, available on <https://seaice.uni-bremen.de>, last access: 30 September 2017, see Fig. S5).

All daily datasets were first averaged to 8-day fields, which are regarded as weekly in this study. The period from the beginning of February to early March comprises four independent weeklong series: week 1 (2–9 February 2015), week 2 (10–17 February 2015), week 3 (18–25 February 2015) and

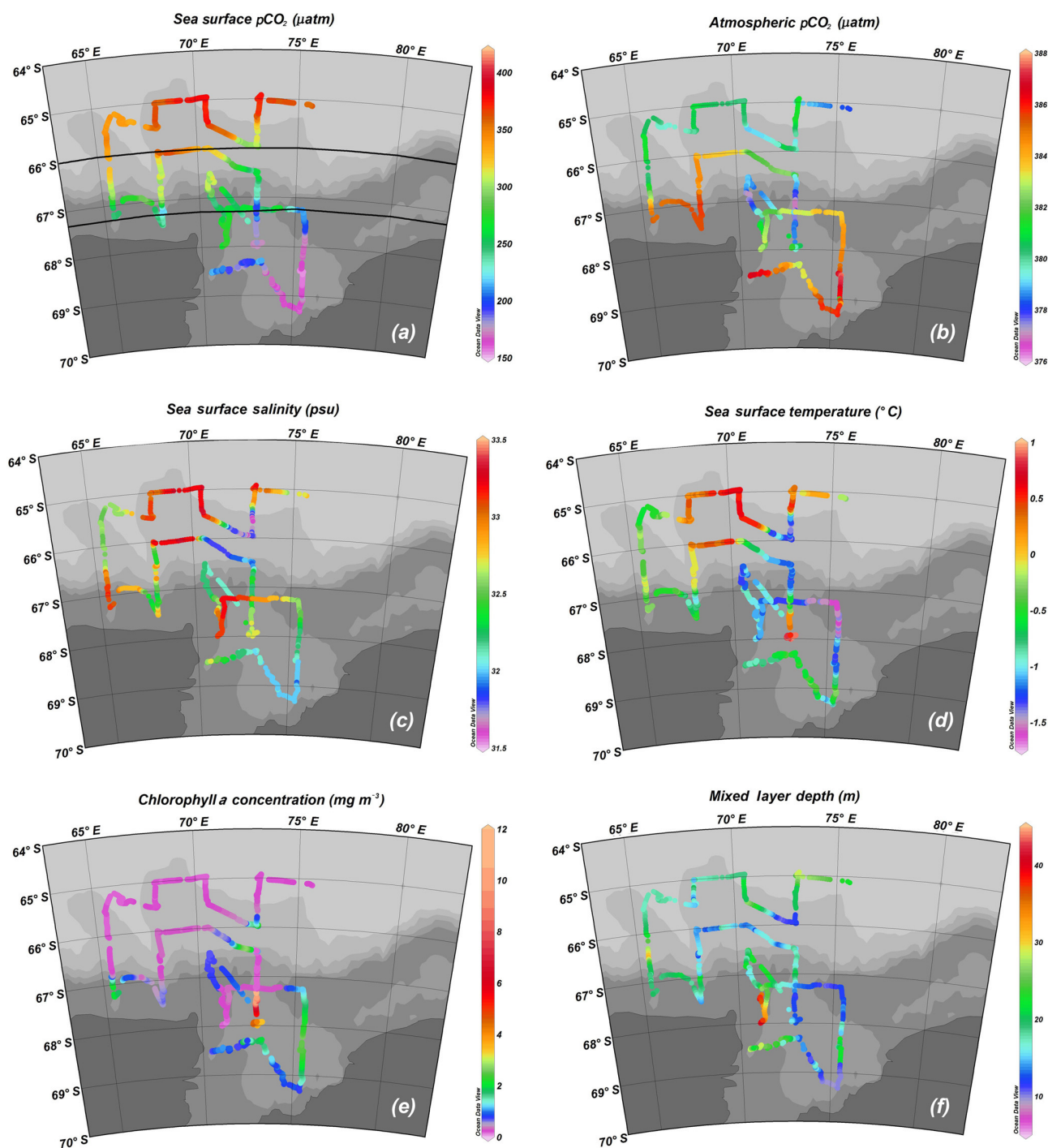


Figure 2. The distributions of underway oceanic and atmospheric $p\text{CO}_2$, SST, SSS and CHL gridded from MODIS, in addition to MLD gridded from station surveys, from February to early March.

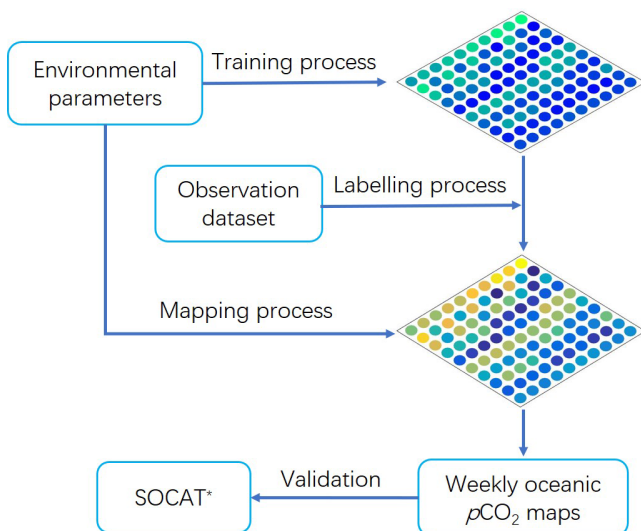
week 4 (26 February–5 March 2015). The weekly proxy parameters (SCMS) were further re-gridded to a horizontal resolution of $0.1^\circ \times 0.1^\circ$ using the kriging method in Surfer software (version 7.3.0.35). In the SOM analyses, input vectors with missing elements are excluded. We compared the assimilated datasets of SST from AVHRR with the in situ measure-

ments obtained by CTD along the cruise. Their correlation is 0.97, and their root mean square error (RMSE) is 0.2°C . Comparing the SSS and MLD fields from the Global Forecast System with the in situ measurements yields correlations of 0.76 and 0.74 and RMSEs of 0.41 psu and 5.15 m, respectively. The uncertainty of the MODIS CHL data in the South-

Table 1. Statistics of labelling and training datasets showing the distribution and coverage of each variable.

Coverage of each variable		SST (°C)	CHL (mg m^{-3})	MLD (m)	SSS (psu)
Labelling	Max	0.81	11.13	40.69	33.81
	Min	-1.44	0.17	7.84	32.43
	Mean	-0.27	3.80	14.41	33.27
	Skewness	0.4 (-0.2) ^a	0.8 (-0.3)	0.9 (0.4)	0.6 (0.6)
Training	Max	2.48	40.17	48.95	34.17
	Min	-1.8	0.06	10.46	28.64
	Mean	-0.53	1.36	14.79	33.16
	Skewness	0.5 (-0.6)	4.3 (0.5)	2.6(0.8)	-0.9 (-1.0)
	N coverage ^b (%)	91.3 (92.5) ^c	82.1 (93.6)	85.0 (98.7)	81.1 (80.4)

^a The skewness of the common logarithm of each variable is shown in parentheses. ^b Number of training data within the labelling data range/total number of training data. ^c The percent labelling data coverage of normalized variables is shown in parentheses.

**Figure 3.** Schematic diagram of the main three steps involved in the SOM neural network calculations used to obtain weekly $p\text{CO}_2$ maps for February to early March 2015.

ern Ocean is approximately 35 % (Xu et al., 2016). For the labelling procedure, the observed oceanic $p\text{CO}_2$ and the corresponding in situ SST, SSS, MLD and MODIS CHL products in vector form are used as the input dataset.

2.3 Validation of SOM-derived oceanic $p\text{CO}_2$

More realistic $p\text{CO}_2$ estimates are expected from SOM analyses when the distribution and variation ranges of the labelling variables closely reflect those of the training datasets (Nakaoka et al., 2013). However, our underway measurements of $p\text{CO}_2$ values have spatiotemporal limitations preventing them from covering the range of variation of the training datasets. To validate the oceanic $p\text{CO}_2$ values reconstructed by the SOM analysis, we used the fugacity of

oceanic CO_2 datasets from the Surface Ocean CO_2 Atlas (hereafter referred to as “SOCAT” data, <http://www.socat.info>, last access: 14 November 2017) version 5 database (Bakker et al., 2016). We selected the dataset from SOCAT (the EXPCODE is 09AR20150128, see cruise in Fig. 4a) that coincided with the same period as our study. The cruise lasted from 6 to 27 February 2015, and $f\text{CO}_2$ measurements were made every 1 min at a resolution of 0.01° . We recalculated $p\text{CO}_2$ values based on the $f\text{CO}_2$ values provided by the SOCAT data using the fugacity correction (Pfeil et al., 2013).

2.4 Carbon uptake in Prydz Bay

The flux of CO_2 between the atmosphere and the ocean was determined using $\Delta p\text{CO}_2$ and the transfer velocity across the sea–air interface, as shown in Eq. (3), where K is the gas transfer velocity (in cm h^{-1}), and the quadratic relationship between wind speed (in units of m s^{-1}) and the Schmidt number is expressed as $(Sc/660)^{-0.5}$. L is the solubility of CO_2 in seawater (in $\text{mol L}^{-1} \text{atm}^{-1}$) (Weiss, 1974). For the weekly estimation in this study, the scaling factor for the gas transfer rate is changed to 0.251 for shorter timescales and intermediate wind speed ranges (Wanninkhof, 2014). Considering the unit conversion factor (Takahashi et al., 2009), the weekly sea–air carbon flux in Prydz Bay can be estimated using Eq. (4):

$$\text{Flux}_{\text{sea-air}} = K \times L \times \Delta p\text{CO}_2 \quad (3)$$

$$\begin{aligned} \text{Flux}_{\text{sea-air}} [\text{gC}/(\text{m}^2 \text{week})] \\ = 30.8 \times 10^{-4} \times U^2 \times (p\text{CO}_2^{\text{sea}} - p\text{CO}_2^{\text{air}}), \end{aligned} \quad (4)$$

where U represents the wind speed 10 m a.s.l. , and $p\text{CO}_2^{\text{sea}}$ and $p\text{CO}_2^{\text{air}}$ are the partial pressures of CO_2 in sea water and the atmosphere, respectively.

We downloaded weekly ASCAT wind speed data (<http://www.remss.com/>, last access: 25 September 2017, see

Table 2. The regional mean values of underway measurements in three subregions.

	$p\text{CO}_2$ (μatm)	SST ($^{\circ}\text{C}$)	CHL (mg m^{-3})	MLD (m)	SSS (psu)
Open-ocean region (66–64° S)	341.48	−0.23	0.45	20.13	32.61
Sea-ice region (66–67.25° S)	276.48	−0.72	0.59	19.44	32.42
Shelf region (67.25–70° S)	198.72	−0.61	1.95	16.84	32.46

Fig. S6) with a resolution of $1/4^{\circ}$ and then gridded the dataset to fit the 0.1° longitude \times 0.1° latitude spatial resolution of the SOM-derived oceanic $p\text{CO}_2$. We gridded the atmospheric $p\text{CO}_2$ data collected along the cruise track to fit the spatial resolution of the SOM-derived oceanic $p\text{CO}_2$ data using a linear method. The total carbon uptake was then obtained by accumulating the flux of each grid in each area according to Jiang et al. (2008) and using the proportion of ice-free areas (Takahashi et al., 2012). When the ice concentration is less than 10 % in a grid, we regard the grid box as comprising all water. When the ice concentration falls between 10 % and 90 %, the flux is computed as being proportional to the water area. In the cases of leads or polynyas due to the dynamic motion of sea ice (Worby et al., 2008), we assume the grid box to be 10 % open water when the satellite sea-ice cover is greater than 90 %.

3 Results and discussion

3.1 The distributions of underway measurements

During austral summer, daylight lasts longer and solar radiation increases. With increasing sea surface temperature, ice shelves break and sea-ice melts, resulting in the stratification of the water column. Starting at the beginning of February, the R/V *Xuelong* sailed from east to west along the sea-ice edge, and its underway measurements are shown in Fig. 2. Based on the water depth and especially the different ranges of oceanic $p\text{CO}_2$ (see Fig. 2a; Table 2), the study area can be roughly divided into three regions, namely, the open-ocean region, the sea-ice region and the shelf region (see Table 2).

The open-ocean region ranges northward from 66 to 64° S, where the Antarctic Divergence Zone is located and water depths are greater than 3000 m. In the open-ocean region, the oceanic $p\text{CO}_2$ was the highest, varying from 291.98 to 379.31 μatm , with a regional mean value of 341.48 μatm . The Antarctic Divergence Zone was characterized by high nutrient concentrations and low chlorophyll concentrations, with high $p\text{CO}_2$ attributed to the upwelling of deep waters, thus suggesting the importance of physical processes in this area (Burkill et al., 1995; Edwards et al., 2004). The

underway sea surface temperatures in this region are relatively high, with an average value of -0.23°C due to the upwelling of Circumpolar Deep Water (CDW), while at the sea-ice edge (73° E, 65.5° S to 72° E, 65.8° S), the SST decreased to less than -1°C . From 67.5° E westward, affected by the large gyre, cold water from high latitudes lowered the SST to less than 0°C . Near the sea-ice edge, SSS decreased quickly to 31.7 psu due to the diluted water; along the 65° S cruise, it reached 33.3 psu; then, moving westward from 67.5° E, affected by the fresher and colder water brought by the large gyre, it decreased to 32.5 psu. The satellite chlorophyll *a* image showed that the regional mean was as low as 0.45 mg m^{-3} , except when the vessel near the sea-ice edge recorded CHL values that increased to 2.26 mg m^{-3} . The lowest $p\text{CO}_2$ value was found near the sea-ice edge due to biological uptake. The distribution of MLD varied along the cruise. Near the sea-ice edge, because of the melting of ice and direct solar warming, a low-density cap existed over the water column, and the MLD was as shallow as 10.21 m. The maximum value of the MLD in the open-ocean region was 31.67 m. In this domain, atmospheric $p\text{CO}_2$ varied from 374.6 to 387.8 μatm . Along the 65° E cruise in the eastern part of the open-ocean region, the oceanic $p\text{CO}_2$ was relatively high, reaching equilibrium with atmospheric $p\text{CO}_2$. In the western part of this region, the oceanic $p\text{CO}_2$ decreased slightly due to the mixture of low $p\text{CO}_2$ from higher latitudes brought by the large gyre. Mixing and upwelling were the dominant factors affecting the oceanic $p\text{CO}_2$ in this domain.

The seasonal sea-ice region (from 66 to 67.25° S) is located between the open-ocean region and the shelf region. In this sector, sea ice changed strongly, and the water depth varied sharply from 700 to 2000 m. The oceanic $p\text{CO}_2$ values ranged from 190.46 to 364.43 μatm , with a regional mean value of 276.48 μatm . Sea ice continued to change and reform from late February to the beginning of March (Fig. 6). The regional mean sea surface temperature decreased slightly compared to that in the open-ocean region, and the average value was -0.72°C . With the rapid changes in sea ice, the sea surface temperature and salinity varied sharply from -1.3 to 0.5°C and from 31.8 to 33.3 psu, respectively. When sea ice melted, the water temperature increased, biological activity increased and the chlorophyll *a* value increased slightly to reach a regional average of 0.59 mg m^{-3} . Due to the rapid change in sea-ice cover, the value of MLD varied from 12.8 to 30.9 m.

The shelf region (from 67.25° S southward) is characterized by shallow depths of less than 700 m, and it is surrounded by the Amery Ice Shelf and the West Ice Shelf. Water inside the shelf region is formed by the modification of low-temperature and high-salinity shelf water (Smith et al., 1984). The Prydz Bay coastal current flows from east to west in the semi-closed bay. The oceanic $p\text{CO}_2$ values in this region were the lowest of those in all three sectors; these values ranged from 151.70 to 277.78 μatm , with a regional average

of $198.72 \mu\text{atm}$. A fresher, warmer surface layer is always present over the bay, which is known as the Antarctic Surface Water (ASW). During our study period, the shelf region was the least ice-covered region. A large volume of freshwater was released into the bay, resulting in a low sea surface temperature (an average of -0.61°C) and salinity (an average of 32.4 psu) values. As shown in Fig. 2f, the MLD in most of the inner shelf is low. Due to the vast shrinking of sea ice and strong stratification in the upper water, algal blooming occurred and chlorophyll values were high, with an average value of 1.93 mg m^{-3} . The chlorophyll a value was remarkably high, reaching 11.04 mg m^{-3} when sea ice retreated in an eastward direction from 72.3°E , 67.3°S to 72.7°E , 68°S . The biological pump became the dominant factor controlling the distribution of oceanic $p\text{CO}_2$. In the bay mouth close to the Fram Bank, due to local upwelling, the water salinity increased remarkably to approximately 33.2 psu .

3.2 Quality and maps of SOM-derived oceanic $p\text{CO}_2$

We selected SOM-derived oceanic $p\text{CO}_2$ values to fit the cruise track of SOCAT for the same period in February 2015 using a nearest-grid method. The RMSE between the SOCAT data and the SOM-derived result was calculated as follows:

$$\text{RMSE} = \sqrt{\frac{\sum (p\text{CO}_2^{\text{sea}}(\text{SOM}) - p\text{CO}_2^{\text{sea}}(\text{SOCAT}))^2}{n}}, \quad (5)$$

where n is the number of validation datasets. The RMSE can be interpreted as an estimation of the uncertainty in the SOM-derived oceanic $p\text{CO}_2$ in Prydz Bay. In this study, the RMSE of the SOM-derived oceanic $p\text{CO}_2$ and SOCAT datasets is $22.14 \mu\text{atm}$, and the correlation coefficient R^2 is 0.82 . The absolute mean difference is $23.58 \mu\text{atm}$. The RMSE obtained in our study is consistent with the accuracies (6.9 to $24.9 \mu\text{atm}$) obtained in previous studies that used neuron methods to reconstruct oceanic $p\text{CO}_2$ (Nakaoka et al., 2013; Zeng et al., 2002; Sarma et al., 2006; Jo et al., 2012; Hales et al., 2012; Telszewski et al., 2009). The precision of this study is on the high side of those that have been previously reported. The slope of the scatterplot indicates that the SOM-derived oceanic $p\text{CO}_2$ data are lower than the SOCAT data (see Fig. 4b). Thus, the precision of these data may have greater uncertainty because the SOCAT dataset does not cover the low- $p\text{CO}_2$ area towards the south. Hence, increasing the spatial coverage of the labelling data will help increase the precision of the SOM-derived oceanic $p\text{CO}_2$.

3.3 Spatial and temporal distributions of SOM-derived oceanic $p\text{CO}_2$

The weekly mean maps of SOM-derived oceanic $p\text{CO}_2$ in Prydz Bay are shown in Fig. 5. In the open-ocean region, the oceanic $p\text{CO}_2$ values were higher than those in the other two regions due to the upwelling of the CDW. During all 4 weeks, this region was nearly ice-free, while the average sea-ice cov-

erage was 18.14% due to the presence of permanent sea ice (see Fig. 6). The oceanic $p\text{CO}_2$ distribution decreased from east to west in the open-ocean region, with lower values observed at the edge of sea ice. In the western part of the open-ocean region, oceanic $p\text{CO}_2$ decreased due to mixing with low oceanic $p\text{CO}_2$ flowing from high-latitude regions caused by the large gyre. From week 1 to week 4, the maximum oceanic $p\text{CO}_2$ increased slightly and reached $381.42 \mu\text{atm}$, which was equivalent to the $p\text{CO}_2$ value of the atmosphere.

In the sea-ice region, sea ice continued to rapidly melt and reform. The weekly mean sea-ice coverage percentage was 29.54% , occupying nearly one-third of the sea-ice region. As shown in Fig. 5, the gradient of the oceanic $p\text{CO}_2$ distribution increased from south to north affected by the flow coming from the shelf region due to the large gyre. In the eastern part of this region, adjacent to the sea-ice edge, the oceanic $p\text{CO}_2$ values were lower. The oceanic $p\text{CO}_2$ changed sharply from $155.86 \mu\text{atm}$ (near the sea-ice edge) to $365.11 \mu\text{atm}$ (close to the open-ocean region).

In austral winter, the entire Prydz Bay basin is fully covered by sea ice, except in a few areas, i.e., the polynyas, which remain open owing to katabatic winds (Liu et al., 2017). When the austral summer starts, due to coincident high wind speeds, monthly peak tides, and/or the effect of penetrating ocean swells, the sea ice in the shelf region starts to melt first (Lei et al., 2010), forming the Prydz Bay polynya. The semi-closed polynya functions as a barrier for water exchange in the shelf region and causes a lack of significant bottom water production, hindering the outflow of continental shelf water and the inflow of Antarctic circle deep water, resulting in the longer residence time of vast melting water and enhanced stratification (Sun et al., 2013). Due to vast melting of the sea ice, the sea surface salinity decreased and algae bloomed; biological productivity promptly increased, and the chlorophyll a concentration reached its peak value. As shown in Fig. 5, the distribution of oceanic $p\text{CO}_2$ in the shelf region was characterized by its lowest values. The obvious drawdown of oceanic $p\text{CO}_2$ occurred in the shelf region due to phytoplankton photosynthesis during this summer bloom. The lowest oceanic $p\text{CO}_2$ in the shelf region was $153.83 \mu\text{atm}$, except at the edge of the West Ice Shelf, where the shelf oceanic $p\text{CO}_2$ exceeded $300 \mu\text{atm}$. The oceanic $p\text{CO}_2$ was the lowest in week 1, which coincided with a peak in chlorophyll a , as evidenced by satellite images. The regional oceanic $p\text{CO}_2$ increased slightly in week 4 compared to the other 3 weeks.

3.4 Carbon uptake in Prydz Bay

During our study period, the entire region was undersaturated, with CO_2 being absorbed by the ocean. The regional averaged ocean–air $p\text{CO}_2$ difference ($\Delta p\text{CO}_2$) was highest in the shelf region, followed by the sea-ice region and the open-ocean region (see Table 3). The regional and weekly mean $\Delta p\text{CO}_2$ in the shelf region changed from

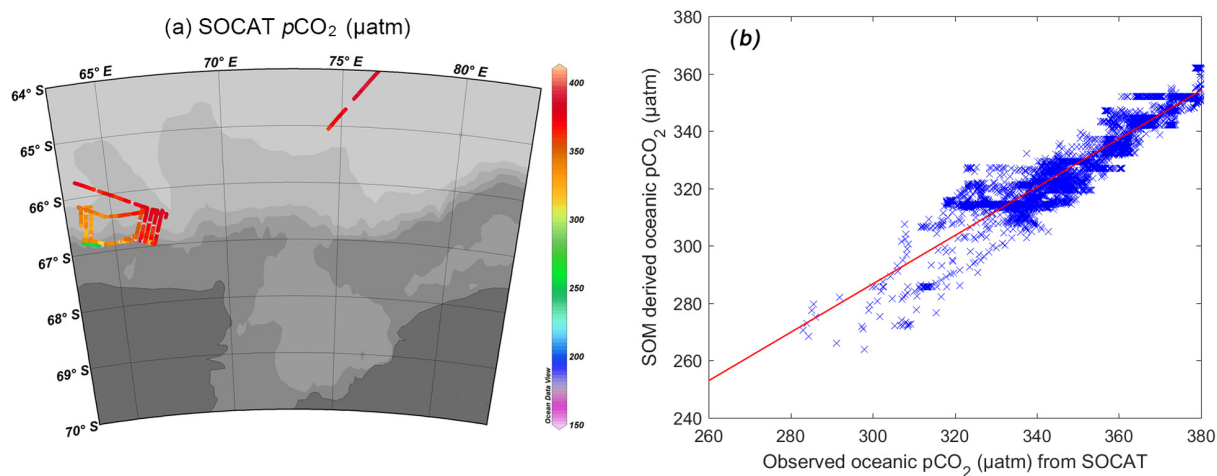


Figure 4. (a) The cruise lines from SOCAT used to validate the SOM-derived oceanic $p\text{CO}_2$ for the study period in 2015; (b) the comparison between the SOM-derived and observed SOCAT oceanic $p\text{CO}_2$ data.

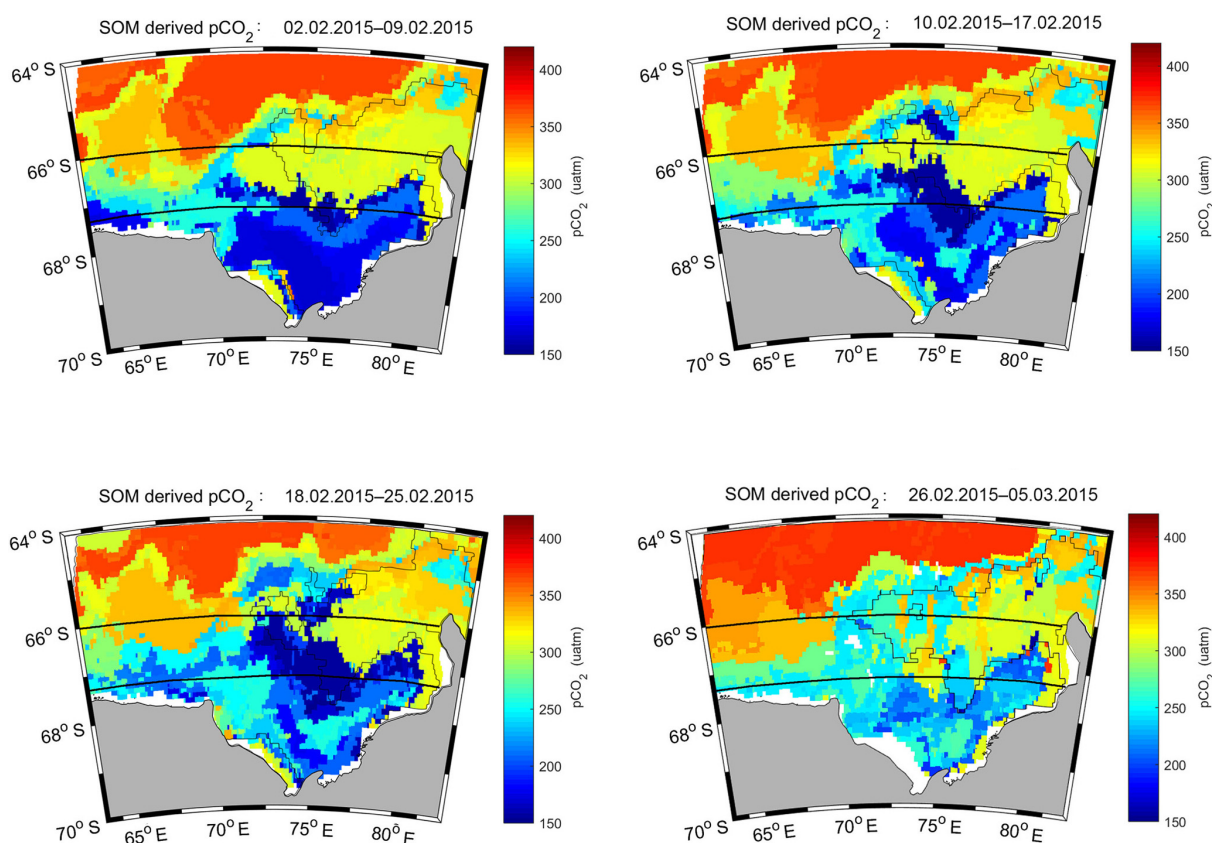


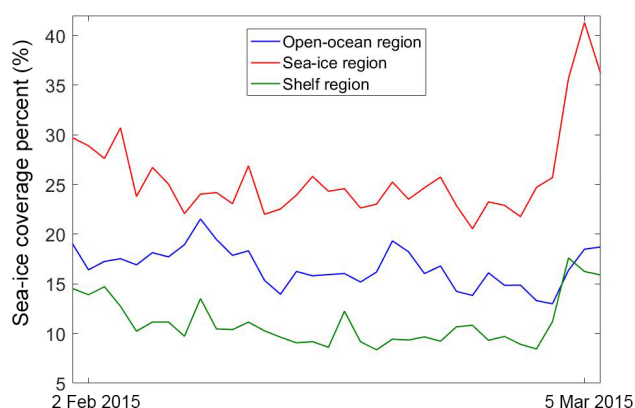
Figure 5. Distribution of weekly mean SOM-derived oceanic $p\text{CO}_2$ in Prydz Bay (in μatm) from 2 February to 5 March 2015. The black contour represents a sea-ice concentration of 15%.

–184.31 μatm in week 1 to –141.00 μatm in week 2 as chlorophyll decreased. The $\Delta p\text{CO}_2$ in the sea-ice region and open-ocean region showed the same patterns, increasing from week 1 to week 3 and then decreasing in week 4. Based on the $\Delta p\text{CO}_2$ and wind speed data, the uptake of CO_2 in

these three regions is presented in Table 3. The uncertainty of the carbon uptake depends on the errors associated with the wind speed, the scaling factor and the accuracy of the SOM-derived $p\text{CO}_2$ according to Eq. (4). The scaling factor will yield a 20% uncertainty in the regional flux estimation.

Table 3. Regional and weekly mean $\Delta p\text{CO}_2$, wind speed and uptake of CO_2 in three subregions (negative values represent directions moving from air to sea).

		Week 1	Week 2	Week 3	Week 4	Uptake in 4 weeks (Tg)
Open-ocean region (66–64° S)	$\Delta p\text{CO}_2$ (μatm)	−34.11	−42.69	−51.94	−34.08	−5.74
	Wind speed (m s^{-1})	7.82	8.54	7.02	9.31	
	Uptake (Tg)	−1.08	−1.55	−1.51	−1.60	
Sea-ice region (66–67.25° S)	$\Delta p\text{CO}_2$ (μatm)	−115.92	−119.83	−127.74	−86.72	−7.82
	Wind speed (m s^{-1})	7.67	8.17	6.39	8.36	
	Uptake (Tg)	−2.11	−2.35	−1.73	−1.63	
Shelf region (67.25–70° S)	$\Delta p\text{CO}_2$ (μatm)	−184.32	−170.23	−158.61	−141.03	−10.01
	Wind speed (m s^{-1})	6.92	7.27	6.67	7.92	
	Uptake (Tg)	−2.51	−2.77	−2.10	−2.63	

**Figure 6.** Percentage of sea-ice coverage in three subregions from 2 February to 5 March 2015 (blue represents the open-ocean region, red represents the sea-ice region and green represents the shelf region).

The errors in the wind speeds of the ASCAT dataset are assumed to be 6 % (Xu et al., 2016); the error in the quadratic wind speed is 12 %. The RMSE of the SOM-derived $p\text{CO}_2$ is 22.14 μatm . Considering the errors described above and the uncertainty occurring when the sea–air computation expression is simplified (1.39 %, Xu et al., 2016), the total uncertainty of the final uptake is 27 %. In the shelf region, the low oceanic $p\text{CO}_2$ levels drove relatively intensive CO_2 uptake from the atmosphere. The carbon uptake in the shelf region changed from week 1 ($2.51 \pm 0.68 \text{ TgC}$, 10^{12} g Tg) to week 2 ($2.77 \pm 0.75 \text{ TgC}$). In contrast, in week 3, the wind speed slowed down, resulting in the uptake of CO_2 in the shelf region decreasing to $2.10 \pm 0.57 \text{ TgC}$. In week 4, even though the $\Delta p\text{CO}_2$ was the lowest of all 4 weeks, the total absorption still increased to $2.63 \pm 0.715 \text{ TgC}$ due to the high wind speed (with an average value of 7.92 m s^{-1}). The total carbon uptake in the three regions of Prydz Bay, integrated from February to early March 2015, was 23.57 TgC , with an uncertainty of $\pm 6.36 \text{ TgC}$.

Roden et al. (2013) estimated coastal Prydz Bay to be an annual net sink for CO_2 of $0.54 \pm 0.11 \text{ mol m}^{-2} \text{ year}^{-1}$, i.e., $1.48 \pm 0.3 \text{ g m}^{-2} \text{ week}^{-1}$. Gibsonab et al. (1999) estimated the average sea–air flux in the summer ice-free period to be more than $30 \text{ mmol m}^{-2} \text{ day}^{-1}$, i.e., $9.2 \text{ g m}^{-2} \text{ week}^{-1}$. Our study suggests that the sea–air flux during the strongest period of the year, i.e., February, could be much larger. The average flux obtained here, $18.84 \text{ g m}^{-2} \text{ week}^{-1}$, is twice as large as the average value estimated over a longer period (November to February) reported by Gibsonab et al. (1999).

As the region recording the strongest surface unsaturation of these three regions in summer, the shelf region has a potential carbon uptake of $10.01 \pm 2.7 \text{ TgC}$ from February to early March, which accounts for approximately 5.0‰–6.7‰ of the net global ocean CO_2 uptake according to Takahashi et al. (2009), even though its total area is only $78 \times 10^3 \text{ km}^2$. Due to the sill constraint, there is limited exchange between water masses in and outside Prydz Bay. During winter, the dense water formed by the ejection of brine in the bay can potentially uptake more anthropogenic CO_2 from the atmosphere that can descend to greater depths, thus enhancing the acidification in deep water. According to Shadwick et al. (2013), the winter pH and Ω values decrease more remarkably than those in summer. As the bottom water in Prydz Bay is a possible source of Antarctic Bottom Water (Yabuki et al., 2006), the shelf region may transfer anthropogenic CO_2 at the surface to deep water; thus, this region may influence the acidification of the deep ocean over long timescales.

4 Summary

Based on the different observed ranges of the distribution of ocean $p\text{CO}_2$, the Prydz Bay region was divided into three sectors from February to early March 2015. In the shelf region, biological factors exerted the main control on oceanic $p\text{CO}_2$, while in the open-ocean region, mixing and upwelling

were the main controls. In the sea-ice region, due to rapid changes in sea ice, oceanic $p\text{CO}_2$ was controlled by both biological and physical processes. SOM is an important tool for the quantitative assessment of oceanic $p\text{CO}_2$ and its subsequent sea–air carbon flux, especially in dynamic, high-latitude, and seasonally ice-covered regions. The estimated results revealed that the SOM technique can be used to reconstruct the variations in oceanic $p\text{CO}_2$ associated with biogeochemical processes expressed by the variability in four proxy parameters: SST, CHL, MLD and SSS. The RMSE of the SOM-derived oceanic $p\text{CO}_2$ is $22.14 \mu\text{atm}$ for the SOCAT dataset. From February to early March 2015, the Prydz Bay region was a strong carbon sink, with a carbon uptake of $23.57 \pm 6.36 \text{ TgC}$. The strong potential uptake of anthropogenic CO_2 in the shelf region will enhance the acidification in the deep-water region of Prydz Bay and may thus influence the acidification of the deep ocean in the long run because it contributes to the formation of Antarctic Bottom Water.

Data availability. CO_2 system data are deposited in the Chinese National Arctic and Antarctic Data center (<http://www.chinare.org.cn/pages/index.jsp>).

Supplement. The supplement related to this article is available online at: <https://doi.org/10.5194/bg-16-797-2019-supplement>.

Author contributions. LC and SX designed the program and YW, DQ, and BL executed the field work. SX and KP analyzed and calculated the data. SX prepared the paper. All authors contributed to discussion and writing.

Competing interests. The authors declare that they have no conflict of interest.

Acknowledgements. This work is supported by the National Natural Science Foundation of China (NSFC41506209, 41630969, 41476172), the Qingdao National Laboratory for marine science and technology (QNL2016ORP0109), the Chinese Projects for Investigations and Assessments of the Arctic and Antarctic (CHINARE2012–2020 for 01–04, 02–01 and 03–04). This work is also supported by Korea Polar Research Institute grant nos. PE19060 and PE19070. We would like to thank the China Scholarship Council (201704180019) and the State Administration of Foreign Experts Affairs P. R. China for their support regarding this research. We would also like to thank the carbon group led by Zhongyong Gao and Heng Sun at GCMAC and the crew of the R/V *Xuelong* for their support on the cruise. We are thankful to contributors to the SOCAT database for validated $p\text{CO}_2$ data and Mercator Ocean for providing the Global Forecast model output. We deeply appreciate Xianmin Hu from the Bedford Institute of Oceanography, who provided us with useful technical instructions.

Edited by: Christoph Heinze

Reviewed by: two anonymous referees

References

- Bakker, D. C. E., Pfeil, B., Landa, C. S., Metzl, N., O'Brien, K. M., Olsen, A., Smith, K., Cosca, C., Harasawa, S., Jones, S. D., Nakaoka, S., Nojiri, Y., Schuster, U., Steinhoff, T., Sweeney, C., Takahashi, T., Tilbrook, B., Wada, C., Wanninkhof, R., Alin, S. R., Balestrini, C. F., Barbero, L., Bates, N. R., Bianchi, A. A., Bonou, F., Boutin, J., Bozec, Y., Burger, E. F., Cai, W.-J., Castle, R. D., Chen, L., Chierici, M., Currie, K., Evans, W., Featherstone, C., Feely, R. A., Fransson, A., Goyet, C., Greenwood, N., Gregor, L., Hankin, S., Hardman-Mountford, N. J., Harlay, J., Hauck, J., Hoppema, M., Humphreys, M. P., Hunt, C. W., Huss, B., Ibáñez, J. S. P., Johannessen, T., Keeling, R., Kitidis, V., Körtzinger, A., Kozyr, A., Krasakopoulou, E., Kuwata, A., Landschützer, P., Lauvset, S. K., Lefèvre, N., Lo Monaco, C., Manke, A., Mathis, J. T., Merlivat, L., Millero, F. J., Monteiro, P. M. S., Munro, D. R., Murata, A., Newberger, T., Omar, A. M., Ono, T., Paterson, K., Pearce, D., Pierrot, D., Robbins, L. L., Saito, S., Salisbury, J., Schlitzer, R., Schneider, B., Schweitzer, R., Sieger, R., Skjelvan, I., Sullivan, K. F., Sutherland, S. C., Sutton, A. J., Tadokoro, K., Telszewski, M., Tuma, M., Van Heuven, S. M. A. C., Vandemark, D., Ward, B., Watson, A. J., and Xu, S.: A multi-decade record of high quality $f\text{CO}_2$ data in version 3 of the Surface Ocean CO_2 Atlas (SOCAT), *Earth Syst. Sci. Data*, 8, 383–413, <https://doi.org/10.5194/essd-8-383-2016>, 2016.
- Barbini, R., Fantoni, R., Palucci, A., Colao, F., Sandrini, S., Ceradini, S., Tositti, L., Tubertini, O., and Ferrari, G. M.: Simultaneous measurements of remote lidar chlorophyll and surface CO_2 distributions in the Ross Sea, *Int. J. Remote Sens.*, 24, 3807–3819, 2003.
- Bates, N. R., Hansell, D. A., Carlson, C. A., and Gordon, L. I.: Distribution of CO_2 species, estimates of net community production, and air-sea CO_2 exchange in the Ross Sea polynya, *J. Geophys. Res.*, 103, 2883–2896, 1998a.
- Bates, N. R., Takahashi, T., Chipman, D. W., and Knapp, A. H.: Variability of $p\text{CO}_2$ on diel to seasonal time scales in the Sargasso Sea, *J. Geophys. Res.*, 103, 15567–15585, 1998b.
- Brainerd, K. E. and Gregg, M. C.: Surface mixed and mixing layer depth, *Deep-Sea Res. Pt. A*, 42, 1521–1543, 1995.
- Burkill, P. H., Edwards, E. S., and Sleight, M. A.: Microzooplankton and their role in controlling phytoplankton growth in the marginal ice zone of the Bellingshausen Sea, *Deep-Sea Res. Pt. II*, 42, 1277–1290, 1995.
- Chen, L., Xu, S., Gao, Z., Chen, H., Zhang, Y., Zhan, J., and Li, W.: Estimation of monthly air-sea CO_2 flux in the southern Atlantic and Indian Ocean using in-situ and remotely sensed data, *Remote Sens. Environ.*, 115, 1935–1941, 2011.
- Chierici, M., Olsen, A., Johannessen, T., Trinanés, J., and Wanninkhof, R.: Algorithms to estimate the carbon dioxide uptake in the northern North Atlantic using ship-observations, satellite and ocean analysis data, *Deep-Sea Res. Pt. II*, 56, 630–639, 2009.
- Chu, P. C. and Fan, C.: Optimal linear fitting for objective determination of ocean mixed layer depth from glider profiles, *J. Atmos. Ocean. Technol.*, 27, 1893–1989, 2010.

- Dandonneau, Y.: Sea-surface partial pressure of carbon dioxide in the eastern equatorial Pacific (August 1991 to October 1992): A multivariate analysis of physical and biological factors, *Deep-Sea Res. Pt. II*, 42, 349–364, 1995.
- Dong, S., Sprintall, J., Gille, S. T., and Talley, L.: Southern Ocean mixed-layer depth from Argo float profiles, *J. Geophys. Res.*, 113, C06013, <https://doi.org/10.1029/2006JC004051>, 2008.
- Edwards, A. M., Platt, T., and Sathyendranath, S.: The high-nutrient, low-chlorophyll regime of the ocean: limits on biomass and nitrate before and after iron enrichment, *Ecol. Model.*, 171, 103–125, 2004.
- Friedrich, T. and Oschlies, A.: Neural network-based estimates of North Atlantic surface $p\text{CO}_2$ from satellite data: A methodological study, *J. Geophys. Res.*, 114, C03020, <https://doi.org/10.1029/2007JC004646>, 2009a.
- Friedrich, T. and Oschlies, A.: Basin-scale $p\text{CO}_2$ maps estimated from ARGO float data: A model study, *J. Geophys. Res.*, 114, C10012, <https://doi.org/10.1029/2009JC005322>, 2009b.
- Gao, Z., Chen, L., and Gao, Y.: Air-sea carbon fluxes and their controlling factors in the Prydz Bay in the Antarctic, *Acta Oceanol. Sin.*, 3, 136–146, 2008.
- Gibson, P. B., Perkins-Kirkpatrick, S. E., Uotila, P., Pepler, A. S., and Alexander, L. V.: On the use of self-organizing maps for studying climate extremes, *J. Geophys. Res.-Atmos.*, 122, 3891–3903, 2017.
- Gibson, J. A. E. and Trull, T. W.: Annual cycle of $f\text{CO}_2$ under sea-ice and in open water in Prydz Bay, east Antarctica, *Mar. Chem.*, 66, 187–200, 1999.
- Hales, B., Strutton, P., Saraceno, M., Letelier, R., Takahashi, T., Feely, R., Sabine, C., and Chavez, F.: Satellite-based prediction of $p\text{CO}_2$ in coastal waters of the eastern North Pacific, *Prog. Oceanogr.*, 103, 1–15, 2012.
- Hardman-Mountford, N., Litt, E., Mangi, S., Dye, S., Schuster, U., Bakker, D., and Watson, A.: Ocean uptake of carbon dioxide (CO_2), MCCIP BriefingNotes, 9 pp., 2009.
- Heil, P., Allison, I., and Lytle, V. I.: Seasonal and interannual variations of the oceanic heat flux under a landfast Antarctic sea ice cover, *J. Geophys. Res.*, 101, 25741–25752, <https://doi.org/10.1029/96JC01921>, 1996.
- Huang, J., Xu, F., Zhou, K., Xiu, P., and Lin, Y.: Temporal evolution of near-surface chlorophyll over cyclonic eddy lifecycles in the southeastern Pacific, *J. Geophys. Res.-Ocean.*, 122, 6165–6179, 2017a.
- Huang, W., Chen, R., Yang, Z., Wang, B., and Ma, W.: Exploring the combined effects of the Arctic Oscillation and ENSO on the wintertime climate over East Asia using self-organizing maps, *J. Geophys. Res.-Atmos.*, 122, 9107–9129, 2017b.
- Iskandar, I.: Seasonal and interannual patterns of sea surface temperature in Banda Sea as revealed by self-organizing map, *Cont. Shelf Res.*, 30, 1136–1148, 2010.
- Jacobs, S. S. and Georgi, D. T.: Observations on the south-west Indian/Antarctic Ocean, in: *A Voyage of Discovery*, edited by: Angel, M., *Deep-Sea Res.*, 24, 43–84, 1977.
- Jamet, C., Moulin, C., and Lefèvre, N.: Estimation of the oceanic $p\text{CO}_2$ in the North Atlantic from VOS lines in-situ measurements: parameters needed to generate seasonally mean maps, *Ann. Geophys.*, 25, 2247–2257, <https://doi.org/10.5194/angeo-25-2247-2007>, 2007.
- Jiang, L. Q., Cai, W. J., Wanninkhof, R., Wang, Y., and Lüger, H.: Air-sea CO_2 fluxes on the US South Atlantic Bight: Spatial and seasonal variability, *J. Geophys. Res.*, 113, C07019, <https://doi.org/10.1029/2007JC004366>, 2008.
- Jo, Y. H., Dai, M. H., Zhai, W. D., Yan, X. H., and Shang, S. L.: On the variations of sea surface $p\text{CO}_2$ in the northern South China sea: A remote sensing based neural network approach, *J. Geophys. Res.*, 117, C08022, <https://doi.org/10.1029/2011JC007745>, 2012.
- Kohonen, T.: *Self-Organization and Associative Memory*, Springer, Berlin, 1984.
- Lafèvre, N., Watson, A. J., and Watson, A. R.: A comparison of multiple regression and neural network techniques for mapping in situ $p\text{CO}_2$ data, *Tellus B*, 57, 375–384, 2005.
- Laruelle, G. G., Landschützer, P., Gruber, N., Tison, J.-L., Delille, B., and Regnier, P.: Global high-resolution monthly $p\text{CO}_2$ climatology for the coastal ocean derived from neural network interpolation, *Biogeosciences*, 14, 4545–4561, <https://doi.org/10.5194/bg-14-4545-2017>, 2017.
- Lei, R., Li, Z., Cheng, B., Zhang, Z., and Heil, P.: Annual cycle of landfast sea ice in Prydz Bay, East Antarctica, *J. Geophys. Res.-Atmos.*, 115, C02006, <https://doi.org/10.1029/2008JC005223>, 2010.
- Liu, C., Wang, Z., Cheng, C., Xia, R., Li, B., and Xie, Z.: Modeling modified circumpolar deep water intrusions onto the Prydz Bay continental shelf, East Antarctica, *J. Geophys. Res.*, 122, 5198–5217, <https://doi.org/10.1002/2016JC012336>, 2017.
- Liu, Y., Weisberg, R. H., and He, R.: Sea Surface Temperature Patterns on the West Florida Shelf Using Growing Hierarchical Self-Organizing Maps, *J. Atmos. Ocean. Technol.*, 23, 325–338, 2006.
- Liu, Z. and Cheng, Z.: The distribution feature of size-fractionated chlorophyll a and primary productivity in Prydz Bay and its north sea area during the austral summer, *Chinese J. Polar Sci.*, 14, 81–89, 2003.
- Liu, Z. L., Ning, X. R., Cai, Y. M., Liu, C. G., and Zhu, G. H.: Primary productivity and chlorophyll a in the surface water on the route encircling the Antarctica during austral summer of 1999/2000, *Polar Res.*, 112, 235–244, 2000.
- Lüger, H., Wallace, D. W. R., Körtzinger, A., and Nojiri, Y.: The $p\text{CO}_2$ variability in the midlatitude North Atlantic Ocean during a full annual cycle, *Global Biogeochem. Cy.*, 18, GB3023, <https://doi.org/10.1029/2003GB002200>, 2004.
- Metzl, N., Brunet, C., Jabaud-Jan, A., Poisson, A., and Schauer, B.: Summer and winter air-sea CO_2 fluxes in the Southern Ocean, *Deep-Sea Res. Pt. I*, 53, 1548–1563, 2006.
- Middleton, J. H. and Humphries, S. E.: Thermohaline structure and mixing in the region of Prydz Bay, Antarctica, *Deep-Sea Res. Pt. A*, 36, 1255–1266, 1989.
- Morrison, J. M., Gaurin, S., Codispoti, L. A., Takahashi, T., Millero, F. J., Gardner, W. D., and Richardson, M. J.: Seasonal evolution of hydrographic properties in the Antarctic circumpolar current at 170 W during 1997–1998, *Deep-Sea Res. Pt. I*, 48, 3943–3972, 2001.
- Nakaoka, S., Telszewski, M., Nojiri, Y., Yasunaka, S., Miyazaki, C., Mukai, H., and Usui, N.: Estimating temporal and spatial variation of ocean surface $p\text{CO}_2$ in the North Pacific using a self-organizing map neural network technique, *Biogeosciences*, 10, 6093–6106, <https://doi.org/10.5194/bg-10-6093-2013>, 2013.

- Nunes Vaz, R. A. and Lennon, G. W.: Physical oceanography of the Prydz Bay region of Antarctic waters, *Deep-Sea Res. Pt. I*, 43, 603–641, 1996.
- Olsen, A., Trinanes, J. A., and Wanninkhof, R.: Sea-air flux of CO_2 in the Caribbean Sea estimated using in situ and remote sensing data, *Remote Sens. Environ.*, 89, 309–325, 2004.
- Pfeil, B., Olsen, A., Bakker, D. C. E., Hankin, S., Koyuk, H., Kozyr, A., Malczyk, J., Manke, A., Metzl, N., Sabine, C. L., Akl, J., Alin, S. R., Bates, N., Bellerby, R. G. J., Borges, A., Boutin, J., Brown, P. J., Cai, W.-J., Chavez, F. P., Chen, A., Cosca, C., Fassbender, A. J., Feely, R. A., González-Dávila, M., Goyet, C., Hales, B., Hardman-Mountford, N., Heinze, C., Hood, M., Hoppema, M., Hunt, C. W., Hydes, D., Ishii, M., Johannessen, T., Jones, S. D., Key, R. M., Körtzinger, A., Landschützer, P., Lauvset, S. K., Lefèvre, N., Lenton, A., Lourantou, A., Merlivat, L., Midorikawa, T., Mintrop, L., Miyazaki, C., Murata, A., Nakadate, A., Nakano, Y., Nakaoka, S., Nojiri, Y., Omar, A. M., Padin, X. A., Park, G.-H., Paterson, K., Perez, F. F., Pierrot, D., Poisson, A., Ríos, A. F., Santana-Casiano, J. M., Salisbury, J., Sarma, V. V. S. S., Schlitzer, R., Schneider, B., Schuster, U., Sieger, R., Skjelvan, I., Steinhoff, T., Suzuki, T., Takahashi, T., Tedesco, K., Telszewski, M., Thomas, H., Tilbrook, B., Tjiputra, J., Vandemark, D., Veness, T., Wanninkhof, R., Watson, A. J., Weiss, R., Wong, C. S., and Yoshikawa-Inoue, H.: A uniform, quality controlled Surface Ocean CO_2 Atlas (SOCAT), *Earth Syst. Sci. Data*, 5, 125–143, <https://doi.org/10.5194/essd-5-125-2013>, 2013.
- Pierrot, D., Neill, C., Sullivan, L., Castle, R., Wanninkhof, R., Lüger, H., Johannessen, T., Olsen, A., Feely, R. A., and Cosca, C. E.: Recommendations for autonomous underway $p\text{CO}_2$ measuring systems and data-reduction routines, *Deep-Sea Res. Pt. II*, 56, 512–522, 2009.
- Rangama, Y., Boutin, J., Etcheto, J., Merlivat, L., Takahashi, T., Delille, B., Frankignoulle, M., and Bakker, D. C. E.: Variability of the net air-sea CO_2 flux inferred from shipboard and satellite measurements in the Southern Ocean south of Tasmania and New Zealand, *J. Geophys. Res.-Ocean.*, 110, 1–17, <https://doi.org/10.1029/2004JC002619>, 2005.
- Roden, N. P., Shadwick, E. H., Tilbrook, B., and Trull, T. W.: Annual cycle of carbonate chemistry and decadal change in coastal Prydz Bay, East Antarctica, *Mar. Chem.*, 155, 135–147, 2013.
- Rubin, S. I., Takahashi, T., and Goddard, J. G.: Primary productivity and nutrient utilization ratios in the Pacific sector of the Southern Ocean based on seasonal changes in seawater chemistry, *Deep-Sea Res. Pt. I*, 45, 1211–1234, 1998.
- Sabine, L., Feely, R. A., Gruber, N., Key, R. M., Lee, K., Bullister, J. L., Wanninkhof, R., Wong, S., Wallace, D. W. R., Tilbrook, B., Millero, F. J., Peng, T.-H., Kozyr, A., Ono, T., and Ríos, A. F.: The oceanic sink for anthropogenic CO_2 , *Science*, 305, 367–371, <https://doi.org/10.1126/science.1097403>, 2004.
- Sarma, V. V. S. S., Saino, T., Sasaoka, K., Nojiri, Y., Ono, T., Ishii, M., Inoue, H. Y., and Matsumoto, K.: Basin-scale $p\text{CO}_2$ distribution using satellite sea surface temperature, Chla, and climatological salinity in the North Pacific in spring and summer, *Global Biogeochem. Cy.*, 20, GB3005, <https://doi.org/10.1029/2005GB002594>, 2006.
- Shadwick, E. H., Trull, T. W., Thomas, H., and Gibson, J. A. E.: Vulnerability of polar oceans to anthropogenic acidification: comparison of Arctic and Antarctic seasonal cycles, *Sci. Rep.*, 3, 2339, <https://doi.org/10.1038/srep02339>, 2013.
- Silulwane, N. F., Richardson, A. J., Shillington, F. A., and Mitchell-Innes, B. A.: Identification and classification of vertical chlorophyll patterns in the Benguela upwelling system and Angola-Benguela front using an artificial neural network, *S. Afr. J. Mar. Sci.*, 23, 37–51, 2001.
- Smith, N. and Tréguer, P.: Physical and chemical oceanography in the vicinity of Prydz Bay, Antarctica, Cambridge University Press, Cambridge, 1994.
- Smith, N. R., Zhaoqian, D., Kerry, K. R., and Wright, S.: Water masses and circulation in the region of Prydz Bay Antarctica, *Deep-Sea Res.*, 31, 1121–1147, 1984.
- Spreen, G., Kaleschke, L., and Heygster, G.: Sea ice remote sensing using AMSR-E 89 GHz channels, *J. Geophys. Res.*, 113, C02S03, <https://doi.org/10.1029/2005JC003384>, 2008.
- Sun, W. P., Han, Z. B., Hu, C. Y., and Pan, J. M.: Particulate barium flux and its relationship with export production on the continental shelf of Prydz Bay, east Antarctica, *Mar. Chem.*, 157, 86–92, 2013.
- Sweeney, C.: The annual cycle of surface water CO_2 and O_2 in the Ross Sea: a model for gas exchange on the continental shelves of Antarctic, *Biogeochemistry of the Ross Sea, Ant. Res. Ser.*, 78, 295–312, 2002.
- Sweeney, C., Hansell, D. A., Carlson, C. A., Codispoti, L. A., Gordon, L. I., Marra, J., Millero, F. J., Smith, W. O., and Takahashi, T.: Biogeochemical regimes, net community production and carbon export in the Ross Sea, Antarctica, *Deep-Sea Res. Pt. II*, 47, 3369–3394, 2000.
- Takahashi, T., Feely, R. A., Weiss, R. F., Wanninkhof, R. H., Chipman, D. W., Sutherland, S. C., and Takahashi, T. T.: Global sea air CO_2 flux based on climatological surface ocean $p\text{CO}_2$, and seasonal biological and temperature effects, *Deep-Sea Res. Pt. II*, 49, 1601–1622, 2002.
- Takahashi, T., Sutherland, S. C., Wanninkhof, R., Sweeney, C., Feely, R. A., Chipman, D. W., Hales, B., Friederich, G., Chavez, F., Sabine, C., Watson, A. J., Bakker, D. C., Schuster, U., Metzl, N., Yoshikawa-Inoue, H., Ishii, M., Midorikawa, T., Nojiri, Y., Körtzinger, A., Steinhoff, T., Hoppema, M., Olafsson, J., Arnarson, T. S., Tilbrook, B., Johannessen, T., Olsen, A., Bellerby, R., Wong, C. S., Delille, B., Bates, N. R., and de Baar, H. J. W.: Climatological mean and decadal change in surface ocean $p\text{CO}_2$, and net sea-air CO_2 flux over the global oceans, *Deep-Sea Res. Pt. II*, 56, 554–577, 2009.
- Takahashi, T., Sweeney, C., Hales, B., Chipman, D. W., Newberger, T., Goddard, J. G., Iannuzzi, R. A., and Sutherland, S. C.: The changing carbon cycle in the Southern Ocean, *Oceanography*, 25, 26–37, 2012.
- Telszewski, M., Chazottes, A., Schuster, U., Watson, A. J., Moulin, C., Bakker, D. C. E., González-Dávila, M., Johannessen, T., Körtzinger, A., Lüger, H., Olsen, A., Omar, A., Padin, X. A., Ríos, A. F., Steinhoff, T., Santana-Casiano, M., Wallace, D. W. R., and Wanninkhof, R.: Estimating the monthly $p\text{CO}_2$ distribution in the North Atlantic using a self-organizing neural network, *Biogeosciences*, 6, 1405–1421, <https://doi.org/10.5194/bg-6-1405-2009>, 2009.
- Thomson, R. E. and Fine, I. V.: Estimating mixed layer depth from oceanic profile data, *J. Atmos. Ocean. Technol.*, 20, 319–329, 2003.
- Ultsch, A. and Röske, F.: Self-organizing feature maps predicting sea levels, *Inform. Sciences*, 144, 91–125, 2002.

- Vesanto, J.: Data Exploration Process Based on the Self-Organizing Map, *Acta Polytechnica Scandinavica, Mathematics and Computing Series*, 115, 96 pp., 2002.
- Wanninkhof, R.: Relationship between wind speed and gas exchange over the ocean revisited, *Limnol. Oceanogr.-Methods*, 12, 351–362, 2014.
- Weiss, R. F.: Carbon dioxide in water and seawater: The solubility of a nonideal gas, *Mar. Chem.*, 2, 201–215, 1974.
- Worby, A. P., Geiger, C. A., Paget, M. J., Van Woert, M. L., Ackley, S. F., and De Liberty, T. L.: Thickness distribution of Antarctic sea ice, *J. Geophys. Res.*, 113, C05S92, <https://doi.org/10.1029/2007JC004254>, 2008.
- Wu, L., Wang, R., Xiao, W., Ge, S., Chen, Z., and Krijgsman, W.: Productivity-climate coupling recorded in Pleistocene sediments off Prydz Bay (East Antarctica), *Palaeogeogr. Palaeoclimatol.*, 485, 260–270, 2017.
- Xu, S., Chen, L., Chen, H., Li, J., Lin, W., and Qi, D.: Sea-air CO_2 fluxes in the Southern Ocean for the late spring and early summer in 2009, *Remote Sens. Environ.*, 175, 158–166, 2016.
- Yabuki, T., Suga, T., Hanawa, K., Matsuoka, K., Kiwada, H., and Watanabe, T.: Possible source of the Antarctic Bottom Water in Prydz Bay region, *J. Oceanogr.*, 62, 649–655, <https://doi.org/10.1007/s10872-006-0083-1>, 2006.
- Zeng, J., Nojiri, Y., Murphy, P. P., Wong, C. S., and Fujinuma, Y.: A comparison of $p\text{CO}_2$ distributions in the northern North Pacific using results from a commercial vessel in 1995–1999, *Deep-Sea Res. Pt. II*, 49, 5303–5315, 2002.
- Zeng, J., Nojiri, Y., Nakaoka, S., Nakajima, H., and Shirai, T.: Surface ocean CO_2 in 1990–2011 modelled using a feed-forward neural network, *Geosci. Data J.*, 2, 47–51, <https://doi.org/10.1002/gdj3.26>, 2015.
- Zeng, J., Matsunaga, T., Saigusa, N., Shirai, T., Nakaoka, S.-I., and Tan, Z.-H.: Technical note: Evaluation of three machine learning models for surface ocean CO_2 mapping, *Ocean Sci.*, 13, 303–313, <https://doi.org/10.5194/os-13-303-2017>, 2017.